Biomaterials Advances 186 (2026) 214913

Contents lists available at ScienceDirect

Biomaterials Advances

journal homepage: www.journals.elsevier.com/materials-science-and-engineering-c

Boronate-crosslinked hyaluronic acid hydrogels with grafting-dependent mechano-redox properties

Maddalena Grieco [a], Sara Maria Giannitelli [b], Ilaria Condò [b], Federico Frateloreto [c], Lorenzo Moroni [a,d], Marcella Trombetta [b], Maria Cristina Cannarsa [e], Giuseppe Gigli [a,g,h], Barbara Cortese [f,g,*], Ornella Ursini [f,**]

[a] National Research Council- Institute of Nanotechnology (CNR Nanotec), c/o Ecotekne, University of Salento, Via Monteroni, 73100, Lecce, Italy
[b] Department of Engineering, Università Campus Bio-Medico di Roma, Via Álvaro del Portillo 21, 00128, Rome, Italy
[c] Department of Chemistry, Sapienza University Rome, Pz.le A. Moro 5, 00185, Rome, Italy
[d] Department of Complex Tissue Regeneration, MERLN Institute for Technology-Inspired Regenerative Medicine, Maastricht University, 6200 MD, Maastricht, the Netherlands
[e] Department of Physics, Sapienza University Rome, Pz.le A. Moro 5, 00185, Rome, Italy
[f] National Research Council- Institute of Nanotechnology (CNR Nanotec), c/o Edificio Fermi, University Sapienza, Pz.le Aldo Moro 5, 00185, Rome, Italy
[g] Tecnomed Puglia - Tecnopolo per la medicina di precisione (Biotech Lecce Hub) c/o Campus Ecotekne, via Monteroni, Lecce, 73100, Italy
[h] Department of Experimental Medicine, University of Salento, Lecce, 73100, Italy

ARTICLE INFO

Keywords:
Dynamic hydrogel
ROS-responsive systems
Dynamic boronic ester covalent bond

ABSTRACT

Reactive oxygen species (ROS) are key regulators of neuronal physiology but contribute to oxidative damage when dysregulated, as in traumatic, ischemic, and inflammatory conditions. Biomaterials capable of replicating the mechanical characteristics of brain extracellular matrix while modulating oxidative stress are therefore of significant interest for neural tissue engineering and in vitro disease modeling. In this study, we functionalized dynamic hyaluronic acid (Ha) hydrogels with 3-aminomethyl phenylboronic acid (PBA) and crosslinked with poly(vinyl alcohol) (PVA) via reversible boronic ester bonds to develop ROS-responsive scaffolds. By varying the degree of PBA grafting, we observed linked feedback governed the mechano-redox properties of Ha-based dynamic hydrogels with the functionalization degree, enabling simultaneous tuning of stiffness, viscoelastic behavior, and antioxidant activity. The developed materials provide a platform for investigating cell responses to mechanically and chemically defined microenvironments and may be useful for modeling oxidative stress–related neuropathological conditions.

1. Introduction

The design of high-quality biomaterials that faithfully mimic the biochemical and mechanical properties of native tissues remains a major challenge in the field of tissue engineering and regenerative medicine field. Within the physiological extracellular matrix (ECM) microenvironment, cells dynamically transduce mechanical cues, ligand-binding dynamics, and biochemical gradients together with redox-mediated signaling driven by reactive oxygen species (ROS). To study the complex cell–matrix interactions that drive cell differentiation and self-assembly in vitro, it is pivotal to replicate the dynamic nature of the native ECM [1,2].

Over the past few years, synthetic biomaterials, particularly polymer-based networks, have emerged as tissue replicates and robust platforms for cell culture. Among these, biopolymer hydrogels [3,4] have attracted increasing attention due to their biochemical and biophysical properties, such as cellular adhesion, degradation, and viscoelasticity. Advances in chemically modified biopolymer hydrogels [5,6] have further expanded their biomedical applications enabling their use in tissue scaffolds, therapeutic delivery systems, tissue adhesives and sealants, as well as interpenetrating network hydrogels. Hydrogels are particularly attractive because they closely replicate the key features of

* Corresponding author at: National Research Council- Institute of Nanotechnology (CNR Nanotec), c/o Edificio Fermi, University Sapienza, Pz.le Aldo Moro 5, 00185, Rome, Italy.
** Corresponding author.
E-mail addresses: barbara.cortese@cnr.it (B. Cortese), ornella.ursini@cnr.it (O. Ursini).

https://doi.org/10.1016/j.bioadv.2026.214913
Received 3 March 2026; Received in revised form 23 April 2026; Accepted 28 April 2026
Available online 30 April 2026

native tissue, where cells naturally reside. The combination of high-water content, softness, flexible structure, transparency, along with tunable chemical and mechanical properties makes them suitable for physiologically relevant scaffolds [7]. Nevertheless, designing scaffolds that accurately mimic the native microenvironment presents challenges, especially in balancing biocompatibility with precise control of biomechanical and biochemical properties [8].

In general, hydrogel polymer networks can be formed through physical or chemical cross-linking. Physically cross-linked networks are stabilized by non-covalent, reversible interactions, but they often lack robustness and long-term stability. In contrast, chemically cross-linked networks rely on covalent bonds, producing elastic gels with higher mechanical strength than physical networks. However, their irreversibility limits applications requiring shear thinning and self-healing behavior.

Dynamic covalent chemistry (DCC) offers an attractive solution to engineer hydrogel networks, allowing the combination of advantageous features of both chemically and physically cross-linked materials [9–11]. Through reversible chemical bonds formed under thermodynamic equilibrium control [12], DCC hydrogels can be tailored to exhibit tunable viscoelasticity, adaptability and self-healing properties [13]. The reversibility of these chemical processes is a key strength in hydrogel design, enabling reversible yet stable bonds that confer unique mechanical properties. Systems based on this chemistry framework exhibit intrinsic adaptability, as their molecular component undergo reversible assembly and disassembly in response to a shift in the chemical equilibrium. Such features make DCC hydrogels attractive for various biomedical applications including tissue engineering, wound dressings and drug delivery [14–17]. Importantly, synthetic dynamic materials that closely mimic the mechanical properties of native tissues also provide valuable tools for understanding how cells sense and remodel their environment. The ability to reversibly tune the mechanical properties of dynamic hydrogels is particularly promising for constructing 3D cell culture scaffolds [18] and for developing biomaterials that mimic the viscoelasticity of soft tissues [19].

Among different chemistries, polysaccharide-based hydrogels cross-linked by boronic acid moieties are emerging as capable of responding to external stimuli and interacting with their environment [20,21]. These dynamic covalent bonds also exhibit self-healing behavior, enabling hydrogels to restore integrity after mechanical damage, chain deformation or chemical degradation. Such properties allow them to mimic the self-healing processes of the human body [22,23]. For example, boronate ester-crosslinking has been shown to yield hydrogels with self-healing behavior under physiological pH [24]. Building on this, phenyl boronic modified hyaluronic acid hydrogels, with good self-healing and tissue adhesion properties, have been designed for use in tissue repair applications [25].

More recently, versatile dynamic hyaluronic acid-based hydrogels based on the boronic ester dynamic covalent bond have been developed as injectable, self-healing, and ROS responsive platforms for tissue engineering, drug/cell delivery, and 3D culture [26]. Among naturally derived polymers, hyaluronic acid (Ha) is particularly promising for the design of such dynamic networks. Ha provides intrinsic biocompatibility and serves as an excellent building block for hydrogels. Its chemical structure allows for various modifications, that adjust cross-linking density, degradability, and dynamic character, making Ha-based hydrogels ideal platforms for studying cellular crosstalk, adhesion and proliferation. A wide range of Ha-based materials has been developed through chemical modification to enhance, modulate, and control their therapeutic potential [27,28]. Notably Ha, as a linear polysaccharide and the only significant glycosaminoglycan component of brain ECM [29,30], is present at high levels in the brain microenvironment under both physiological and pathological conditions, including neural injury, stroke, inflammation, and tumor progression, highlighting its relevance as a biomaterial platform [8,31,32]. In particular, following neural injury, the local microenvironment undergoes dramatic biochemical changes that influence tissue repair and regeneration. Among these changes, oxidative stress which is driven by the excessive accumulation of ROS, creates a toxic milieu and contributes to neuronal dysfunction [33].

These ROS are primarily generated as by-products of mitochondrial respiration, and their accumulation leads to oxidative stress, cellular damage, and mitochondrial dysfunction [34]. Increased ROS levels further amplify injury by promoting the release of inflammatory mediators that trigger neuronal apoptosis and necrosis, generated both during mitochondrial respiration and on the membranes of neutrophils and phagosomes via NADPH oxidase [35].

Incorporating ROS-responsive or ROS-scavenging functionality into hydrogel scaffolds represents a powerful strategy to better recapitulate the neural microenvironments subjected to oxidative stress and provide therapeutic benefits beyond structural support. Hydrogels capable of responding to or neutralizing ROS can, not only mitigate oxidative stress–induced cytotoxicity but also create a more favorable milieu for neural survival, proliferation, and regeneration. Thus, reducing ROS generation or actively scavenging ROS represents a critical therapeutic goal in regenerative biomaterial design.

This study models oxidative stress conditions relevant to neuronal environments that remain highly relevant, though not exclusive, to traumatic, ischemic, and inflammatory conditions [36]. Here, we report the design of dynamic, ROS-responsive hyaluronic acid hydrogels functionalized with 3-aminomethyl phenylboronic acid (PBA) and crosslinked with poly(vinyl alcohol) (PVA) through reversible boronic ester bonds. By tuning the degree of PBA grafting, we modulated the hydrogel's mechanical, rheological, and antioxidant properties to mimic the viscoelasticity of brain tissue while actively scavenging ROS. The resulting Ha–PBA–PVA hydrogels were comprehensively characterized to elucidate the relationship between grafting degree, mechanical behavior, antioxidant performance, and neuronal cell response. Aligned with the SH-SY5Y neuron-like model and preserving translational relevance across multiple neuropathological contexts, this framework supports the development of a multifunctional platform for the study of neuron-like oxidative stress and the implementation of redox-active neurodegenerative strategies.

2. Materials and methods

2.1. Materials

Hyaluronic acid sodium salt (MW 1500–2200 kDa) was purchased from Acros Organics with a 95% purity; 3-aminomethyl phenyl-boronic acid hydrochloride (3-aminomethyl PBA) was purchased from Santa Cruz Biotechnology; 4-(4,6-dimethoxy-1,3,5-triazine-2-yl)-4-methylmorpholinium chloride (DMTMM) was purchased from Toronto Research Chemicals, as a coupling agent.

Ha with a high MW was selected as a reproducible high-molecular-weight commercial grade to ensure sufficient viscoelasticity and chain entanglement for stable hydrogel formation [37].

Polyvinyl alcohol (PVA, Mw 13,000-23,000, purity 98%) was purchased from Sigma Aldrich. The dialysis membrane Spectra-Por 7 MWCO 10 kDa was purchased from Spectrum Labs (San Francisco Bay Area, CA, USA).

2.2. Synthesis of functionalized Ha with 3-aminomethyl PBA group: Ha-PBA polymer

Hyaluronic acid (Ha) was functionalized on the side chain with phenyl-boronic groups (3-aminometyl phenyl boronic acid, PBA) as briefly described: sodium hyaluronate was completely dissolved in DI water (0.5% *w/v* solution) under constant stirring at room temperature (RT). Subsequently, DMTMM and 3-aminomethyl PBA were added under constant stirring at RT. DMTMM and 3-aminomethyl PBA were added in different ratios compared to Ha, to obtain various degrees of

chemical functionalization of Ha chain (grafting). The reaction was carried out for 72 h under strict control of the pH, which was kept around 6.5–7 with NaOH 1 M. The reaction mixture was consequently transferred to a dialysis membrane (6–8 kDa molecular weight cut-off) and dialysed against DI water for about four days at RT. The system was kept in a constant gentle agitation, and the water was changed twice a day to allow complete removal of the low-molecular-weight impurities. Finally, the resulting solution was frozen at −80 °C for 24 h, lyophilized and then stored at RT until use. The purified product was recovered via freeze-drying and characterized using ^{1}H NMR.

2.3. Proton nuclear magnetic resonance ^{1}H NMR characterization of Ha-PBA polymer

The degree of functionalization with PBA group was measured at room temperature using a proton nuclear magnetic resonance (^{1}H NMR) with a Bruker AVANCE III 400 MHz. The Ha-PBA polymer samples were dissolved in D_2O. The degree of substitution was determined by the ratio of the integral of aromatic protons from the conjugated phenylboronic acid group (between 7.5 ~ 8 ppm, -C_6H_4) to the integral of the Ha methyl proton peak (at 2.0 ppm, -CH_3) (Fig. S1 and S2).

2.4. Formation of dynamic Ha-PBA-PVA hydrogel: Boronic ester bond formation as dynamic bond

The dynamic boronic ester hydrogel was formed through the condensation reaction between a boronic group and the OH-diols groups (cis-1,3 diols) of polyvinyl alcohol (PVA) (Fig. 2). The reaction took place in aqueous solutions under RT without the requirement of a catalyst [38] by solubilizing the PVA solution at the desired amount on a magnetic stirrer at a temperature above 80 °C. The protocol consisted of preparing the two different solutions and then gently mixing them. The Ha-PBA solution, was simply obtained by dissolving the synthesized product in the right solvent (phosphate buffer PBS or H2O deionized) at the chosen weight/volume ratio at RT.

The final hydrogel network is the result of dynamic bond formation between the PBA groups present in Ha-PBA and the -OH diols groups (cis-1,3-diols) present in PVA [38].

2.5. Mechanical properties of hydrogel Ha-PBA-PVA

Cylindrical samples (Ø = 8 mm, h = 4 mm) were compressed at a crosshead speed of 1 mm/min up to 50% strain by using a universal testing machine (model 3365, Instron Corporation, Issaquah, WA, USA) equipped with a 10 N load cell. A load/unload cycle was recorded for each sample. The compressive modulus was calculated as the slope of the linear region of the stress–strain curves (corresponding to 5–15% strain). Each experiment was carried out in triplicate.

2.6. Rheological characterization of hydrogel Ha-PBA-PVA

To characterize the viscoelastic behavior of this dynamic hydrogel, rotational tests were performed with an Automatic MCR 302 rheometer (Anton Paar), equipped with PP 25 (parallel plate, 25 mm diameter) and a measuring gap of 0.5 mm. Hydrogel samples (500 μL) were prepared in 2 mL Eppendorf tubes and then transferred to the lower plate of the measuring system. Viscosity curves were obtained via rotational tests preset in shear rate (velocity preset mode) with values of $\gamma^{\cdot} = 0.1–100$ s-1.

2.7. Self-healing properties of hydrogel Ha-PBA-PVA

To characterize the self-healing ability of Ha-PBA based hydrogel, a beam-shaped compression test was performed [22]. In brief, hydrogel samples were prepared directly in a polydimethylsiloxane (PDMS) mold to give them a cylindrical shape (Fig. S3a) (4 mm height, 8 mm diameter, 240 μL) and were left to rest for 24 h inside it to obtain uniform hydrogels. Samples both clear and stained with rhodamine (1% *w/v*) samples were fabricated. To stain the hydrogel, a small amount of dye (about 2% *v*/v) was dropped into the PVA solution immediately before mixing it with Ha-PBA to enable crosslinking. Then, cylindrical samples were cut in two with a razor and two semi-circular parts (one clear and one stained) were placed in contact and allowed to heal for 6 and 24 h, at RT (inside a 35 mm petri dish to limit evaporation). The Healing Efficiency (HE) [%] was calculated as the ratio between compressive load at breaking point of the healed sample over the original one (as a percentage). Using a uniaxial tensile testing machine (Instron 3365, equipped with a 10 N load cell) the beam-shaped compression test was performed on original, 6 h and 24 h healed specimens. The beam-shaped compression upper element was obtained by printing the support with an Ender-3 (Creality) 3D printer in poly lactic acid (PLA) and using a needle (1.8 mm diameter) as the beam (Fig. S3b and Fig. S3c). Each test was performed with the beam imprinting on the healing line and by setting a compression rate of 1 mm/s and an end-of-test condition (maximum strain of 90%) via Bluehill software. Compressive load/strain curves were derived. Each experimental condition was repeated three times.

2.8. Swelling

The hydrogel samples (100 μL) were produced as described above and their initial weights were recorded (W_0). For in vitro swelling tests, the hydrogels were fully immersed in PBS solution and high and low glucose medium for complete swelling. The test was carried out at RT for eight days and the swelled weight (W_S) of each sample was measured approximately every day. The swelling ratio was calculated according to the following equation

$$Swelling\% = \frac{W_s - W_0}{W_0} \bullet 100$$

2.9. $^{\bullet}O_2^-$ radical scavenging properties

The pyrogallol autooxidation method was used to evaluate the superoxide anion $\bullet O_2^-$radical-scavenging activity [39,40]. Briefly, a solution 100 mM pyrogallol was prepared by dissolving it in a 10 mM HCl solution. The scavenging properties of Ha-PBA polymer were then tested by individually mixing 30 μL of each solution of Ha-PBA 2% w/vol in PBS with 120 μL Tris−HCl (50 mM, pH = 7.5) in a 96-well plate, and by subsequently adding 15 μL of pyrogallol solution (100 mM in HCl [10 mM]) into the mixture. To test the scavenging properties of the hydrogel, 10 μL of PVA solution was added to 30 μL of Ha-PBA (2% w/vol in PBS) to guarantee hydrogel formation. Then, 160 μL Tris−HCl (50 mM, pH = 7.5) and 20 μL of pyrogallol solution (100 mM in HCl [10 mM]) was subsequently added into each well of a 96-well plate.

In the control group, 30 μL or 40 μL of DI water was added instead of the precursor solution. Each group had 3 replicates. The absorbance was measured using a TECAN Infinite M Nano $^{+}$plate reader. The ability to scavenge superoxide radicals on superoxide radicals at 320 nm was calculated using equation:

$$\text{scavenging effect}\% = [(A_0 - A_S)/A_0] \times 100$$

where A_0 is the absorbance of the control where PBS was added instead of the samples and A_S is the absorbance of the samples.

2.10. $^{\bullet}OH$ radical scavenging properties

The Fenton reaction was employed to determine the scavenging effect of hydrogels on hydroxyl radical generation.

To assess the $^{\bullet}$OH radical scavenging ability, the Ha-PBA grafted polymer and the corresponding Ha-PBA-PVA hydrogels (of different degrees of grafting 46% and 69%) were incubated in a solution of H_2O_2

(1 mM), $FeCl_2$ (0.2 mg/mL), and methylene blue (0.01 mg/mL) for at least 1 h. The volumes of Fenton reagent and methylene blue were adjusted according to the volume of the Ha-PBA or hydrogel solutions, ensuring that the volumes ratio remained constant. The hydroxyl radical ($^{\bullet}OH$) scavenging activity of the hydrogel was studied using methylene blue (MB) as the $^{\bullet}OH$ indicator probe. After incubation with ferrous ions (Fe^{2+}) and H_2O_2 solution (1 mM), the colour of MB solution rapidly turned from dark- blue to pale blue, indicating $^{\bullet}OH$ generation. The inhibiting/ scavenging effect on hydroxyl radicals was calculated using the equation modified from ref. [41].

Scavenging effect (%) = (A_{sample}-A_{blank})/ ($A_{control} - A_{blank}$) *100.

The inhibiting/scavenging effect was calculated using the absorbance at 655 nm.

The blank group contained methylene blue and Fenton reagent [H_2O_2 + ferrous ions (Fe^{2+}) solution].

The control group comprised methylene blue without oxidative reagent. The sample groups contained Ha-PBA grafted polymer or the Ha-PBA-PVA hydrogels, methylene blue and Fenton reagent. Subsequently, the solution was measured at a wavelength range of 400–800 nm by a UV–Vis spectrophotometer (TECAN Infinite M Nano+ plate reader) to evaluate the ROS levels.

2.11. Cell culture

Human neuroblastoma cells (SH-SY5Y, a cloned subline of neuroblastoma cell line from a metastastic bone tumor) were cultured at 37 °C in a humidified atmosphere with 5% CO_2 and expanded in Dulbecco's modified Eagles medium high glucose (DMEM; Gibco, Berlin), supplemented with 10% (*v*/v) heat-inactivated fetal bovine serum (FBS; Gibco), 1% penicillin–streptomycin (P/S; Gibco) and 1% L-glutamine (Gibco). Cells were detached from the substrate with Trypsin/EDTA (Corning) and suspended in media at a cellular concentration of 3×10^6 cell/mL hydrogel. Cells below passage 20 were used in order to avoid cell senescence.

Hydrogels Ha-PBA-PVA (using Ha-PBA at 46% and 69% grafting degree) were prepared for all biological experiments in 96-well plates, in a 3:1 ratio of Ha-PBA to PVA. Briefly, 20 μL of cell suspension with appropriate cell concentration was added to 75 μL of Ha-PBA (2%) solution. The two solutions are gently mixed with the help of a 10 μL tip and then 25 μL of PVA (1%) was added to the mixture without further mixing. Subsequently, 100 μL of Low-Glucose DMEM (Gibco) was added to the formed hydrogels. All biological experiments were conducted at 24 h, 48 h and 72 h, at least in triplicate.

2.12. Metabolic activity assay

The metabolic activity was evaluated using MTS assays, according to the manufacturer's instructions. Hydrogels were prepared in 96-well plates as previously described. After 24 h, 48 h and 72 h the medium was discarded and 100 μL of MTS solution was added. Cells were incubated at 37 °C for 2 h, and then the formazan crystals were extracted from the cells with a solubilizing solution (DMSO). The optical density (OD) was measured at 490 nm, using a microplate reader (Glomax Discovery). The experiments were conducted at 24 h, 48 h and 72 h, at least in triplicate.

2.13. Propidium iodide staining

PI staining of SH-SY5Y cells embedded in the hydrogels was carried out as previously reported [42]. Cell viability was observed at 10× magnification under a confocal microscope (Zeiss LSM 980). The analyses were performed by assessing the number of cells positive for both dyes and calculating the ratio of live cells to total cells (L/(L + D)). The experiments were conducted at 24, 48 and 72 h, at least in triplicate.

2.14. Intracellular ROS analyses

Intracellular ROS levels were measured using 2,7-dichlorofluorescein diacetate (DCFH-DA; Sigma-Aldrich, 35845) according to the manufacturer's instructions. SH-SY5Y cells embedded in the hydrogel were also stained using DAPI. The ROS levels were observed at 10× magnification under a confocal microscope (Zeiss LSM 980). The analysis was performed by calculating the ratio of fluorescence intensity induced by the DCFH-DA and normalized to the number of live cells. The experiments were conducted at 24 h, 48 h and 72 h, at least in triplicate.

2.15. Statistical analysis

Statistical analysis was performed with GraphPad Prism 9.0 (GraphPad Software, Inc., San Diego, CA). The values are expressed as mean ± S.E.M. for 3 or more independent experiments. Statistical differences were determined using unpaired *t*-tests (two-tailed), Mann–Whitney *U* tests (two-tailed), One-way ANOVA with Tukey multiple-comparison test. A *p*-value of less than 0.05 ($p < 0.05$) was considered statistically significant for all tests. The significance levels were considered as follows: $^{****}p < 0.0001$, $^{***}p < 0.001$, $^{**}p < 0.01$, and $^{*}p < 0.05$.

3. Results and discussion

3.1. Synthesis of Ha-PBA polymer and dynamic hydrogel formation Ha-PBA-PVA

The chemical functionalization of Ha to obtain Ha-PBA conjugate was achieved through a one-step synthesis process, grafting the 3-aminomethyl PBA moiety to the Ha backbone to achieve different degrees of chemical functionalization of the Ha chain. DMTMM was used as the coupling agent to activate the carboxyl groups of Ha to form the Ha-PBA amide bond. The amount of DMTMM and 3-aminomethyl-PBA was systematically calculated to guarantee different ratios compared to Ha, as reported in Table 1.

As shown in Fig. 1, the synthesis of Ha functionalized with 3-aminomethyl-PBA group is a condensation reaction between the carboxyl groups of Ha and the amine groups of 3-aminomethyl PBA, with the formation of a strong covalent bond, as the amide bond. The reaction took place in aqueous solutions under room temperature and it did not require the use of a catalyst [38].

To establish the degree of chemical functionalization of Ha, ^1H NMR analyses were performed. The NMR spectra of Ha-PBA polymers for the two different syntheses (Fig. S1 and S2 in SI), showed that the chemical functionalization of Ha with 3-aminomethyl-PBA groups was strongly dependent on the molar ratio 3-aminometil-PBA/Ha and on the molar ratio DMTMM/Ha. In fact, increasing the amount of DMTMM in the conjugation reaction raised the grafting ratio and resulted in 69% of the PBA moiety being grafted in the Ha backbone.

3.2. Dynamic hydrogel characterization

The dynamic hydrogel Ha-PBA-PVA was prepared mixing the Ha-PBA solution and the PVA solution together (Fig. 2).

Gelation occurred rapidly due to the formation of the boronic ester bond formation [9,10,20,38,43–49] as a dynamic bond. As the physicochemical properties of the Ha-PBA-PVA hydrogel depend on various factors such as the degree of functionalization of Ha with the 3-aminomethyl PBA chemical group, the concentration of each hydrogel component, (i.e. Ha-PBA solution concentration and PVA solution concentration), the volume ratio between Ha-PBA solution and PVA solution and the nature of the solvent used in the preparation of the Ha-PBA and PVA solutions, we functionalised Ha with different grafting degrees, respectively 46% and 69% (referred as Ha-PBA_{46}-PVA hydrogel and Ha-PBA_{69}-PVA hydrogel) as reported in Table 2. Ha-PBA and PVA were

Table 1
Reaction conditions to achieve different degrees of grafting of the Ha chain. The grafting degree was determined by NMR analyses.

Ha (g)	Ha (mmol)	3-aminomethyl-PBA (mmol)	DMTMM (mmol)	Molar ratio 3-aminomethyl-PBA/ Ha	Molar ratio DMTMM/Ha	Chemical Yield (%)	Grafting degree
1.99836	4.996	2.993	4.946	0.599	0.99 *ca* equimolar compared to Ha	95.4	46%
0.37568	0.939	0.941	2.822	1.002	3.00	100	69%

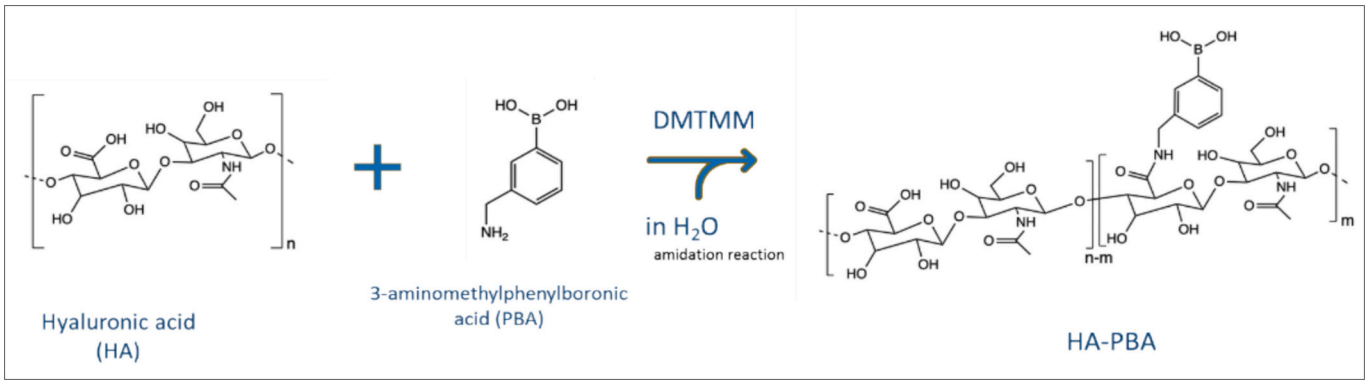

Fig. 1. Scheme of chemical functionalization of Ha with 3-aminometyl phenyl boronic acid (PBA): synthesis of Ha-PBA polymer.

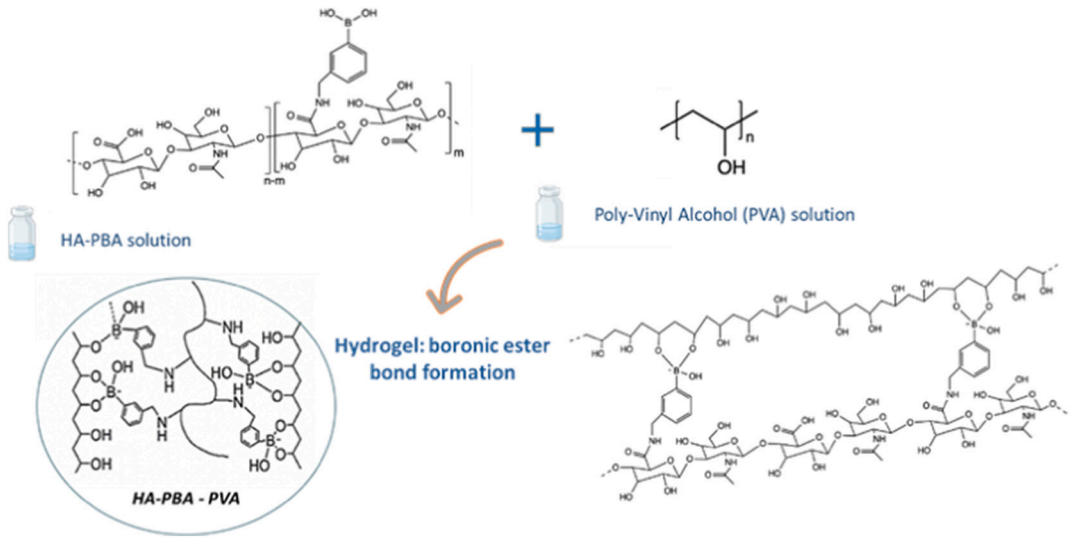

Fig. 2. Scheme of the reactions that result in hydrogel formation and molecular structure of the hydrogel.

Table 2
Compositions of hydrogels formed by combination of Ha-PBA solutions and PVA solution.

Ha-PBA $_{(\%grafting)}$ + PVA	Concentration weight/vol (in PBS)	Ha-PBA/PVA ratio in PBS (vol/vol)
Ha-PBA $_{46}$	Ha-PBA: 2% PVA: 1%	3:1
Ha-PBA $_{69}$	Ha-PBA: 2% PVA: 1%	3:1

dissolved in PBS (pH 7.4), also considering the sensitivity of boron bonds to pH changes [9].

3.3. Mechanical properties of the Ha-PBA-PVA hydrogel

The mechanical behavior of the hydrogels in response to increasing stress was investigated through a compression test and evaluated by the stress-strain curve, as shown in Fig.S4. The elastic modulus (Young's modulus) of the Ha-PBA_{69}-PVA hydrogel was 3.88 ± 1.04 kPa, significantly higher than that of the Ha-PBA_{46}-PVA hydrogel which was 1.12 ± 0.24 kPa (Fig. 3a).

This suggested that the increased number of PBA functional groups on Ha promoted the formation of more dynamic boronic ester bonds when interacting with PVA. Consequently, the Ha-PBA_{69}-PVA hydrogel, with a higher grafting degree was correspondingly stiffer. Given that the Young's modulus of cerebral tissue is slightly above 1 kPa [50], hydrogels designed to mimic this stiffness are particularly important for influencing and determining cell fate. Brain tissue exhibits a remarkably soft mechanical profile, with reported elastic moduli typically ranging from ~0.1 to 2 kPa depending on the anatomical region and measurement technique [51–54]. In this context, the mechanical properties of the developed hydrogels fall within a physiologically relevant range. In

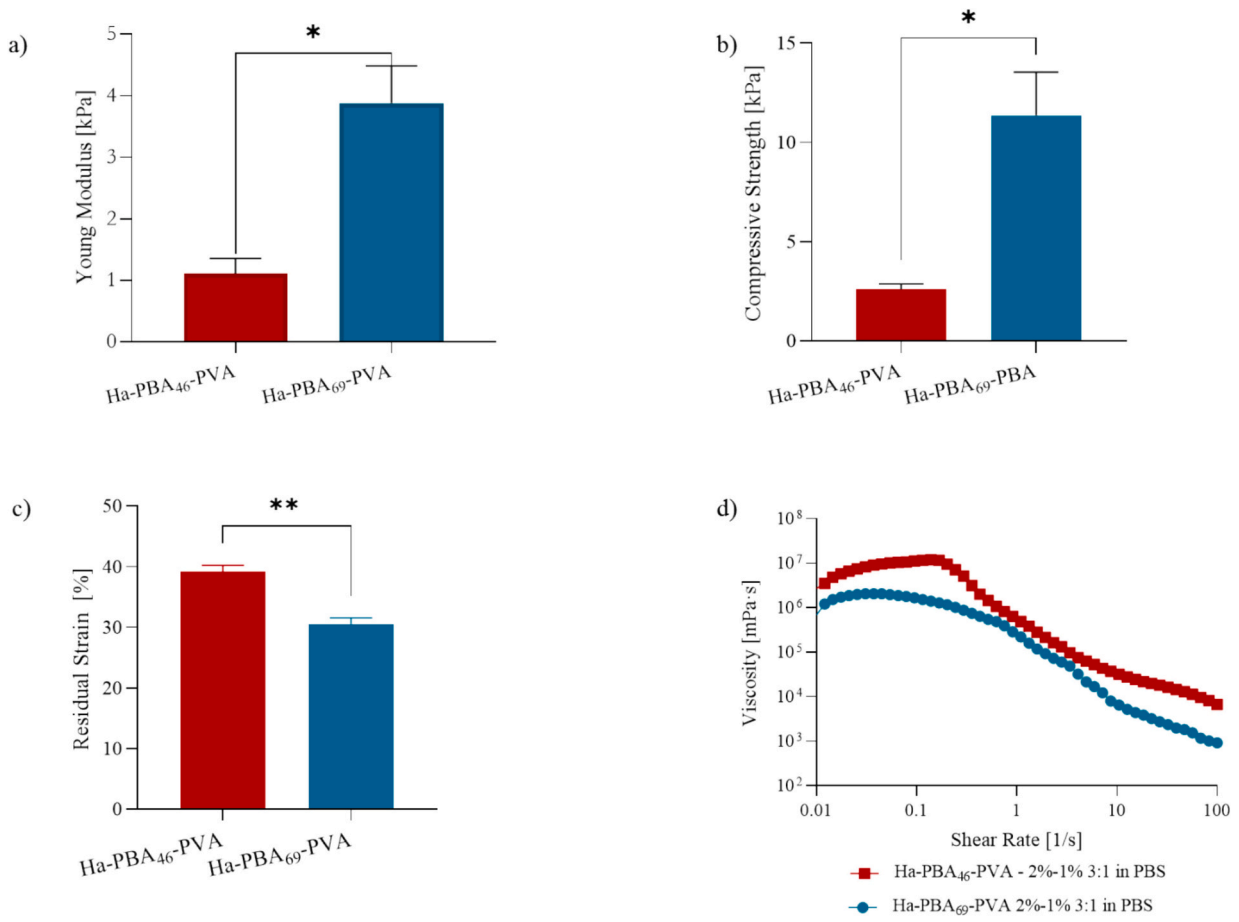

Fig. 3. Mechanical behavior of Ha-PBA-PVA hydrogels with different grafting degrees: a) Young Moduli; b) Compressive strength; c) Residual strain d) Viscosity curves of Ha-PBA_{69}-PVA and Ha-PBA_{46}-PVA hydrogels. The values are the mean ± s.e.m. of three independent experiments. * indicates statistically significant differences using unpaired *t*-test with * $p < 0.05$, ** $p < 0.01$.

particular, the Ha-PBA_{46}-PVA hydrogel (≈1.12 kPa) closely matches the stiffness of native brain tissue, while the Ha-PBA_{69}-PVA hydrogel (≈3.88 kPa) provides a moderately stiffer yet still compliant microenvironment. This tunability enables the recreation of distinct mechanical niches, allowing investigation of how subtle variations in stiffness influence neuronal behavior under physiologically and pathologically relevant conditions.

Furthermore, the stress-strain curves obtained from the compression tests on the hydrogels (Fig. S4), indicate that the Ha-PBA_{69}-PVA hydrogel exhibited a higher maximum compressive stress than the Ha-PBA_{46}-PVA hydrogel (Fig. 3b). This trend is consistent with the corresponding Young's moduli, confirming that an increase in the degree of grafting leads to a stiffer network that can withstand higher loads.

In addition, the residual deformation, after unloading, decreased with the increase of the grafting degree. Specifically, the Ha-PBA_{46}-PVA hydrogel showed a higher residual strain (Fig. 3c), indicating reduced elastic recovery and increased viscoelastic dissipation.

The viscosity of the Ha-PBA-PVA hydrogels was evaluated by a shear-rate-controlled rotational test (Fig. 3d). For both Ha-PBA_{69}-PVA and Ha-PBA_{46}-PVA hydrogels, viscosity decreased with the increasing of the shear rate, indicating a shear-thinning behavior. The viscosity of the Ha-PBA-PVA hydrogels with Ha-PBA_{69} and Ha-PBA_{46} grafting, were 1.79×10^6 and 8.77×10^6 mPa·s, respectively (Fig. 3d).

The reported values were taken at the minimum shear rate, approximating rest conditions.

The lower viscosity observed for the Ha-PBA_{69}-PVA hydrogel relative to Ha-PBA_{46}-PVA is consistent with the corresponding residual strain values, indicating that Ha-PBA_{69}-PVA hydrogel can recover its initial shape more easily.

These differences can be attributed to the incorporation of the dynamic 3-aminomethyl PBA moiety, which alters the polymer molecular structure and, consequently, the mechanical properties of hydrogels. At higher grafting degrees, a greater number of reversible crosslinks are formed, which can readily dissociate and reform under shear, facilitating network rearrangement.

Consequently, the Ha-PBA_{69}-PVA hydrogel displays lower viscosity under shear, a desirable feature for injectable and self-healing hydrogel systems. Furthermore, the viscosity value reflects the hydrogel composition in terms of the Ha-PBA content (*w/v*%). Indeed, the viscosity increased from 2.23×10^6 mPa·s to 8.77×10^6 mPa·s as the Ha-PBA_{46} concentration increased from 1% to 2% (*w/v*), keeping the 3:1 *v*/v ratio with the 1% PVA solution constant (Fig. S5).

Our viscosity values are of the same order of magnitude as those reported by Duan et al., where viscosities of 1.035×10^6 mPa·s and 2.275×10^6 mPa·s were obtained [38]. It should be noted that our hydrogels were prepared by mixing a 2 wt% Ha-PBA solution with a 1 wt % PVA solution and that the grafting degree of our Ha-PBA is greater than that reported in the literature (34%). This suggests that the viscosity values are strongly influenced by the grafting of the 3-aminomethyl PBA moiety bonded to the Ha backbone.

3.4. Swelling and stability

The swelling process, namely the ability to increase and retain the amount of water within the network, depends on the structure of the hydrogel and the degree of cross-linking.

As expected, due to the higher number of dynamic bonds present within the Ha-PBA$_{69}$-PVA hydrogel, a lower swelling capacity of the hydrogel with a higher grafting was observed (Fig. 4a). As the ability of hydrogels to form and heal can be influenced by interactions with the components present in the cell culture medium [49], due to the high reactivity of boronic acids with diols which allows interaction with a range of saccharides we also investigated the swelling behavior in different media.

Boronic acid-functionalized hydrogels are renowned for being glucose-responsive due to the reversible interaction between boronic acid and cis–diol–containing molecules, such as glucose. Therefore, a glucose-dependent swelling measurement was carried out on the Ha-PBA$_{46}$-PVA hydrogel (Fig. 4b). The resistance to swelling decreased with the increase of glucose levels [55,56] as the PBA moieties formed dynamic boronate ester bonds with the free glucose molecules present in the surrounding medium, resulting in a decrease in the number of crosslinks within the hydrogel network. This reduced crosslinked network led to increased hydrophilicity and osmotic pressure inside the matrix, allowing a higher water uptake and consequently hydrogel swelling which caused the volumetric change [57].The Ha polymer backbone, modified with 3-aminophenylboronic acid, reversibly bound free glucose in solution, resulting in a hydrogel through the formation of a bis-bidentate bond [58]. Although only the Ha-PBA$_{46}$-PVA hydrogel was examined, the results indicated that the reversible boronate–diol interactions are sufficient to modulate the hydrogel network in response to glucose. It is expected, however, that varying the degree of grafting would influence the magnitude and rate of swelling, as higher PBA contents provide more binding sites for glucose and thus a higher swelling ratio. Overall, our results indicate a glucose-binding capacity of the PBA.

3.5. Self-healing properties of the hydrogel

The quantitative estimation of the healing ability of the hydrogels, was evaluated using a beam-shaped compression test [59]. After 6 h, the superior healing efficiency of Ha-PBA$_{69}$-PVA can be attributed to the higher density of reversible dynamic bonds, which can readily dissociate and reform, thereby facilitating efficient repair and enhancing short-term healing performance (Fig. 5).

Extending the healing time to 24 h, the HE approached to 100% for both hydrogels, indicating that within a single day, each hydrogel was able to completely recover to its original properties. The lower healing efficiency of the Ha-PBA$_{46}$-PVA hydrogel observed after 6 h may be attributed to its higher viscosity, which likely slows the healing process.

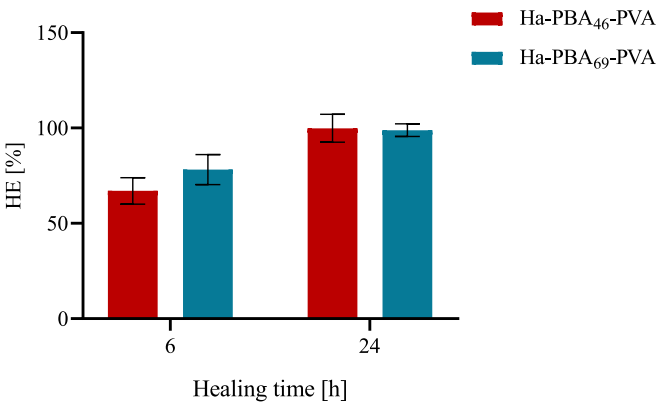

Fig. 5. Healing efficiency of the Ha-PVA-PBA hydrogel (after healing for 6 and 24 h at room temperature). Statistical differences were determined using unpaired *T*-Test (Prism 8.01).

3.6. $^{\bullet}O_2^-$ radical scavenging properties of Ha-PBA polymers and Ha-PBA-PVA hydrogels

Under conditions of oxidative stress in neural microenvironments and other inflamed or metabolically compromised tissues, the imbalance between the generation and elimination of ROS leads to redox dysregulation, cellular dysfunction, lipid peroxidation, and damage to biomacromolecules [33]. In this context, ROS-responsive hydrogels, particularly boronate ester-based Ha systems, represent innovative platforms for buffering oxidants and reshaping the pericellular redox landscape, integrating structural support with chemical reactivity [60]. To explore the ability of the Ha-PBA-PVA hydrogels to scavenge superoxide anion radicals ($^{\bullet}O_2^-$) the pyrogallol autoxidation assay was used to measure the inhibition of pyrogallol autoxidation catalyzed by the superoxide radical [39–41,61]. During the pyrogallol autooxidation process, the chromophore purpurogallin compound is formed, exhibiting a characteristic UV absorption maximum at 320 nm. The addition of $^{\bullet}O_2^-$ radical-scavenging agent inhibits the pyrogallol autoxidation, thereby reducing purpurogallin production and consequently decreasing absorbance at 320 nm. In our experiments, neither Ha nor PVA showed measurable radical-scavenging activity, as their UV absorbance profiles remained higher than that of the control sample (Fig. 6a – 6b). These results indicated that both the Ha and PVA systems do not act as a scavenger for the $^{\bullet}O_2^-$ radical anion. Whereas, the UV–Vis curves of the Ha-PBA-PVA hydrogels (Fig. 6c) showed an absorbance profile lower than the curve of the control sample and independent of the grafting degree. These results indicated that the hydrogels exhibit an effective oxygen-radical scavenging capacity (Fig. 6d) and that the $^{\bullet}O_2^-$ radical scavenging ability is not affected by the polymer grafting degree.

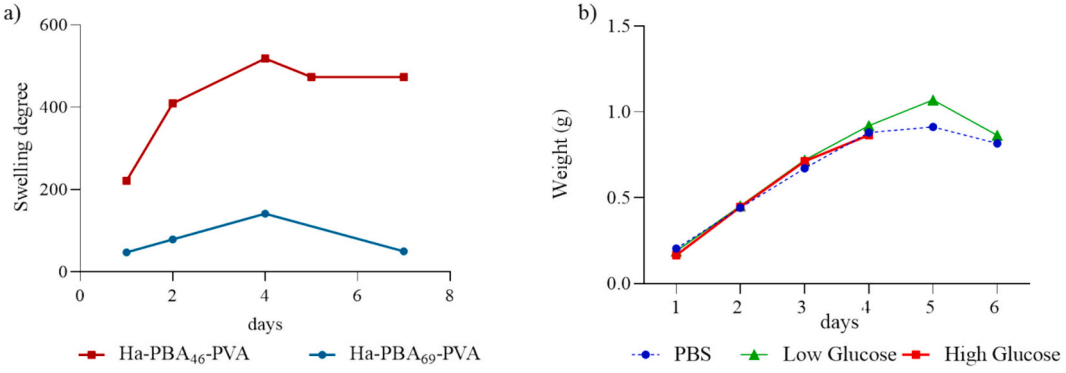

Fig. 4. a) Swelling profiles of hydrogels Ha-PBA$_{46}$-PVA and Ha-PBA$_{69}$-PVA in PBS. b) Swelling behavior of the Ha-PBA$_{46}$-PVA hydrogel as a function of solvent nature.

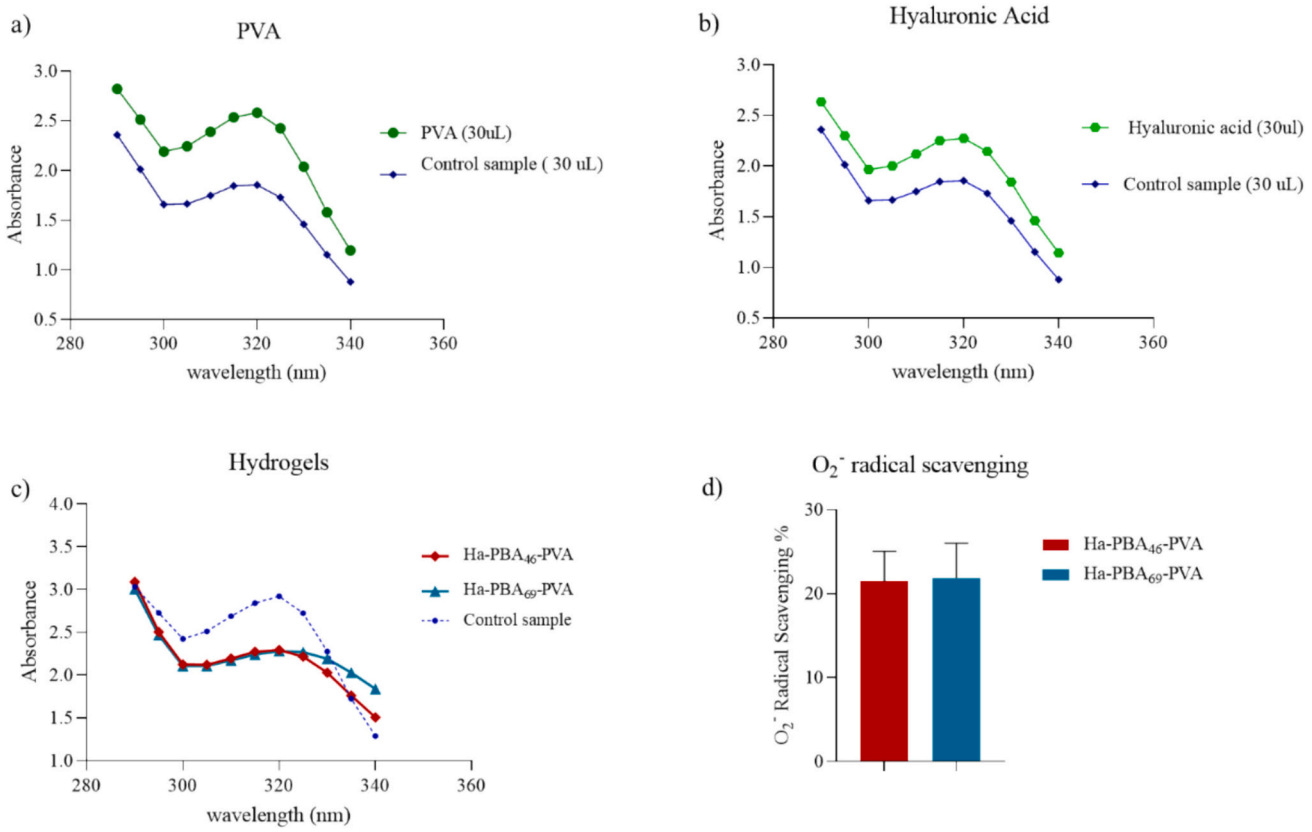

Fig. 6. UV–Vis curve determined by pyrogallol assay of: a) pure PVA polymer; b) UV–Vis curve of pure hyaluronic acid (Ha) and c) UV–Vis curve of Ha-PBA-PVA hydrogels. d) Bar graph quantifying the superoxide radical anion scavenging effect of Ha-PBA-PVA hydrogels determined at 320 nm. The values are the mean ± s.e. m. of three independent experiments.

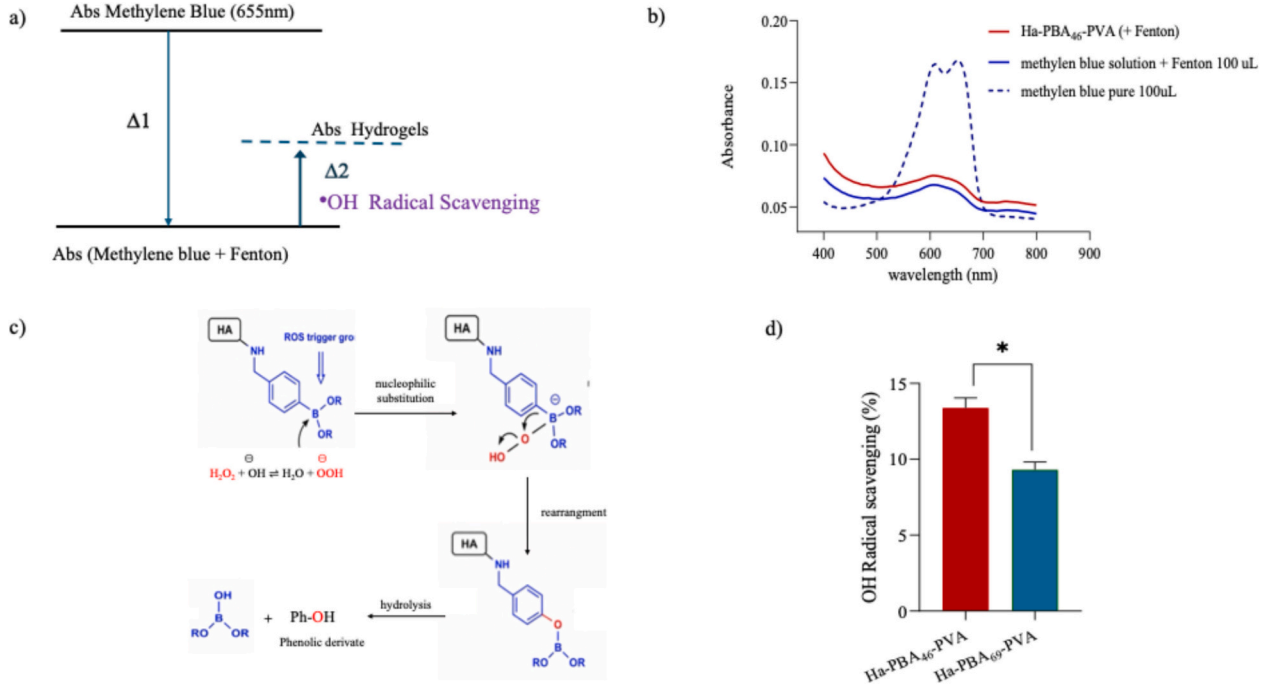

Fig. 7. a) Schematic representation of how the change of methylene blue absorbance induced by the Fenton reaction, used to quantify radical scavenging activity. b) Changes in the UV spectrum of the oxidative degradation of methylene blue in presence of the hydrogel. c) Mechanism scheme of OH radical scavenging of phenylboronate d) Bar graph quantifying the •OH scavenging ability of Ha-PBA-PVA hydrogels using the Fenton degradation MB method. The values are the mean ± s.e. m. of independent experiments. * Statistical differences were determined using unpaired *t*-test (Prism 8.01).

3.7. •OH radical scavenging properties of Ha-PBA polymers and Ha-PBA-PVA hydrogels

Hydroxyl radical •OH is one of the most reactive and severe among ROS, able to damage cellular systems such as DNA, proteins and lipids [62]. To determine the hydroxyl radical scavenging properties of the Ha-PBA-PVA hydrogels, we performed the Fenton assay, an advanced oxidation process consisting of H_2O_2 and ferrous ions for the generation of hydroxyl radicals (•OH) [41]. The hydroxyl radical produced by the catalytic decomposition of H_2O_2 produces the oxidative degradation of methylene blue. This thiazine dye is used to track the generation of •OH radicals [63,64]. The changes in the UV spectrum of methylene blue during its oxidative degradation are shown in Fig. S6, resulting in a decrease of absorbance due to the oxidative degradation of methylene blue dye.

As shown in Fig. 7b, the presence of hydrogels that act as •OH radical scavengers, significantly mitigated the Fenton-induced decrease in absorbance, resulting in a comparatively higher absorbance profile. This behavior indicates that the hydrogels effectively neutralize hydroxyl radicals generated during the Fenton reaction. The quantitative scavenging ability of the hydrogels is shown in Fig. 7d. The radical-scavenging behavior of the hydrogels can be attributed to the presence of phenylboronic moieties within the polymeric network. Phenylboronic acid groups are well known to be responsive to hydrogen peroxide and other ROS. The underlying mechanism shown in Fig. 7c, involves the oxidative conversion of the boronic group. Upon exposure to ROS, the phenylboronic acid moiety is oxidized at the boron center, generating a tetrahedral intermediate that subsequently undergoes a rearrangement involving 1,2-migration of the phenyl group from boron to oxygen, generating a borate species. The latter is subsequently hydrolyzed to yield the corresponding phenolic derivative. [36,65,66]. Thus, this ROS-triggered transformation accounts for the observed attenuation of hydroxyl radical activity in the system. Hydrogels with a lower grafting degree (Ha-PBA_{46}-PVA hydrogel) exhibited higher scavenging ability, indicating that the extent of boronate-ester bonds obtained with PVA, directly affects the •OH scavenging abilities. As the extent of dynamic bond formation increases, the number of active sites available to quench radicals correspondingly decreases. A higher degree of dynamic boronate-ester linkages, as in the Ha-PBA_{69}-PVA hydrogel, resulted in a proportional reduction in the accessible reactive sites required for effective radical neutralization.

Similar observations have been reported in previous studies, in which boronic acid hydrogels exhibited a pronounced H_2O_2 responsive behavior. In such systems, the B—C bond within the boronic moiety is susceptible to oxidative cleavage in the presence of H_2O_2, leading to hydrogel degradation and thereby imparting H_2O_2-responsiveness to the system [67]. Compared with previously reported Ha–PBA systems [25], our Ha-PBA-PVA hydrogels demonstrated moderate scavenging efficiencies. Overall, our findings confirm that the Ha-PBA-PVA hydrogels endows the system with notable antioxidant potential. This property may be beneficial for mitigating oxidative stress in biomedical applications particularly in environments characterized by elevated ROS levels.

3.8. Functionalization of Ha-PBA modulates ROS generation in a neuroblastoma cell line

Although ROS are normal metabolic products of cells, their excessive accumulation increases the oxidative stress in surrounding tissues, leading to the exacerbation of inflammation. To assess the intrinsic ROS-scavenging ability of the Ha-PBA-PVA hydrogels, a DCFH-DA assay was performed using SH-SY5Y cells (Fig. 8). Confocal microscopy results showed that intracellular ROS levels were stable for cells encapsulated in Ha-PBA_{46}-PVA hydrogels. This behavior was associated to the presence of fewer boronic acid moieties available for oxidation, making it less effective in modulating ROS levels, resulting in sustained oxidative stress within the cultured cells. On the other hand, Ha-PBA_{69}-PVA hydrogels significantly reduced the ROS levels in SH-SY5Y cells over time, indicating that a higher degree of grafting provided a greater density of reactive sites capable of neutralizing intracellular ROS, in the cellular microenvironment.

Previous reports showed that controlled scavenging of extracellular oxidants supports the maintenance of redox-regulated signaling pathways and preserves neuronal metabolic integrity [68,69]. Consistently, the higher PBA grafting in Ha-PBA_{69}-PVA showed that initially, increasing of the density of oxidation-susceptible arylboronic groups within the hydrogel network, enhanced the system's capacity to consume chemically reactive species, such as ROS, and reduced the exposure of encapsulated cells to oxidants. Taken together these findings are consistent with previous reports demonstrating that the redox capacity of boronate-containing biomaterials is directly proportional to the density of reactive groups and plays a pivotal role in shaping the cellular response [70,71].

3.9. PBA grafting influences cellular viability and metabolic activity

The ability of PBA-modified hydrogels to regulate ROS is particularly relevant because oxidative stress is a key determinant of cellular fate.

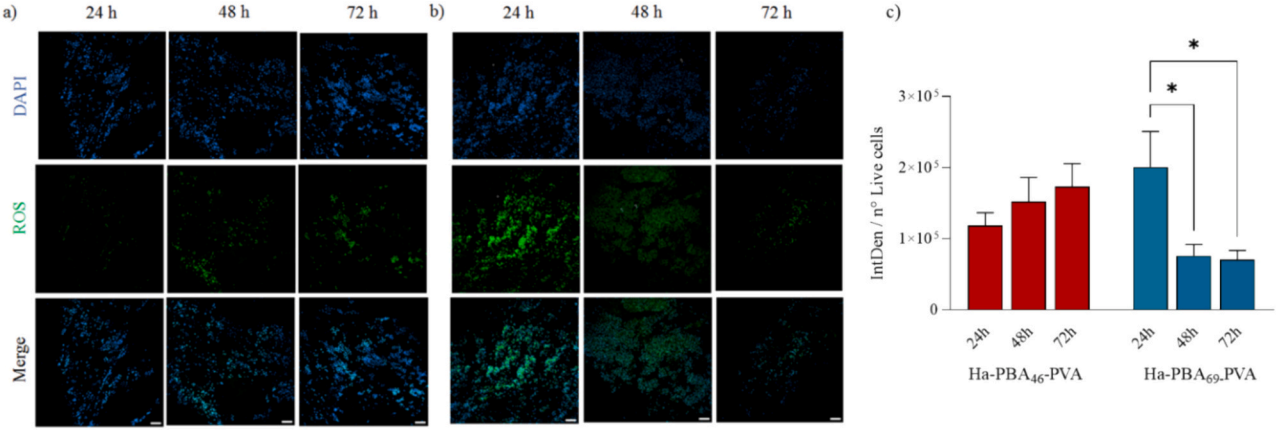

Fig. 8. ROS production in SH-SY5Y cells encapsulated in Ha-PBA hydrogels of 46% and 69% grafting degree. a-b) Representative confocal image of ROS production in SH-SY5Y cell line encapsulated in a) Ha-PBA_{46}-PVA hydrogels and b) Ha-PBA_{69}-PVA hydrogels over 24, 48 and 72 h, where all cells were counterstained with DCFH-DA (green) and DAPI (blue). Scale bar: 100 μm. c) Quantification of ROS levels measured by DCFH-DA, after 24 h, 48 h and 72 h. The values are the mean ± s.e.m. of three independent experiments. * indicates statistically significant difference using one-way ANOVA and Mann Whitney test with * $p < 0.05$.

Physiological levels of ROS function as essential second messengers that support proliferation, metabolic activity and signaling pathways, whereas sustained or excessive ROS accumulation triggers oxidative damage, mitochondrial dysfunction, and apoptosis [72]. Maintaining ROS at signaling-permissive levels preserves redox-regulated survival programs and prevents the transition to distress-associated bioenergetic dysfunction [68,73]. To evaluate the biocompatibility of Ha-PBA-PVA with different grafting degrees, a Live/Dead assay was performed using the SH-SY5Y cells encapsulated within the hydrogel matrices (Fig. 9 a-c), from 1 to 3 days. Quantitative analysis of cell viability calculated by comparing the number of live cells to the total number of cells, revealed a strong dependence on the degree of grafting. Cells encapsulated in Ha-PBA$_{46}$-PVA hydrogels showed, over time, a stable viability, indicative of a non-expanding population consistent with either low-proliferative behavior or a division–loss equilibrium, whereas cells encapsulated in Ha-PBA$_{69}$-PVA hydrogels showed a consistently higher percentage of viable cells (Fig. 9c). These findings are in agreement with studies on Ha-boronate systems which demonstrated that integrating arylboronic groups into Ha/PVA networks enabled oxidant-responsive tuning of the microenvironment with measurable biological gains [26], and that cell viability was influenced by variations in Ha–PBA concentration at a constant grafting density. Our results, therefore, confirm a comparable trend. In particular, the reduced cell proliferation observed at higher PBA concentrations may be attributed to the presence of an excess of PBA within the hydrogel network. An elevated PBA content could exert an inhibitory effect on cellular growth, potentially by interfering with cellular metabolic processes or membrane-associated interactions. Such effects are consistent with the hypothesis that elevated levels of phenylboronic acid may disrupt cellular homeostasis, thereby limiting proliferation under these conditions. To further validate the biocompatibility results, the metabolic activity of cells was assessed using an MTS assay (Fig. 9d). We observed a stable metabolic activity in Ha-PBA$_{46}$-PVA hydrogels over 3 days, which corresponded to a constant number of viable cells over time. This stability suggested a preserved mitochondrial function in a population that does not undergo net expansion. On the other hand, Ha-PBA$_{69}$-PVA hydrogels showed a reduced cellular metabolic activity after 24 h, which remained consistent up to 72 h. This apparent decrease coincided with an increase in the total number of viable cells over time, suggesting that the metabolic activity per cell was reduced as the cell number increased. The MTS assay determines cellular viability through metabolic activity, reflecting the activity status of the mitochondria. We, thus, hypothesised that encapsulation of SH-SY5Y cells in the hydrogels induced a lag phase in cellular activity, as cells have to adapt to a stiffer microenvironment, where proliferation outpaces the metabolic demand [74,75]. The increased rigidity of the extracellular environment (as in the Ha-PBA$_{69}$-PVA hydrogels) in fact, forced the cells to undergo an initial adaptation phase and the formation of clustered cell zones (Fig. 9b), causing stress during the adaptation phase. Interestingly, after this initial adaptation phase, the presence of increased cell-cell cross-talk favored the proliferation and stabilization of the mitochondrial machinery. Despite temporal stability, the Ha-PBA$_{46}$-PVA hydrogels network fails to support proliferative expansion, likely because of limited ROS buffering, weak adhesion reinforcement, and attenuated mechanotransduction which did not allow to generate the redox and mechanical cues necessary for cell-cycle commitment and growth (Fig. 9d). However, cells

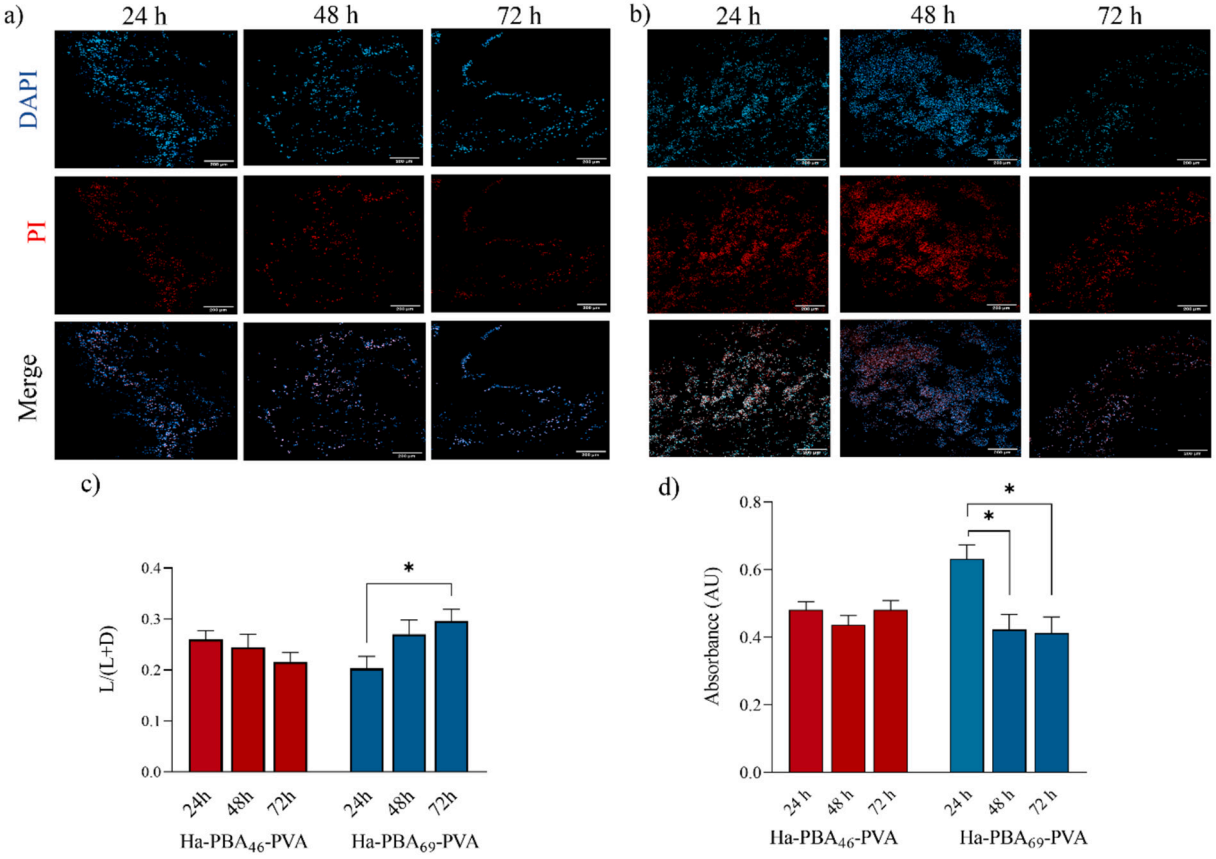

Fig. 9. Biocompatibility of SH-SY5Y seeded on Ha-PBA hydrogels with functionalization rates of 46% and 69% show a dependency on the degree of grafting. a-b) Representative confocal images of SH-SY5Y cells encapsulated in a) Ha-PBA$_{46}$ -PVA and b) Ha-PBA$_{69}$-PVA hydrogels after 1, 3, 7 days of growth Cells were stained with DAPI (blue), for visualization of all nuclei and with propidium iodide, PI (red) for visualization of dead cells. Scale bar 200 μm. c) Quantification of live cells to total cells (L/(L + D). d) Metabolic activity of SH-SY5Y cells after 24, 48 and 72 h cultured on hydrogels (46% and 69%). Data are shown as mean ± s.e.m. of three independent biological experiments. * indicates statistically significant difference using one-way ANOVA and Mann-Whitney test with * $p < 0.05$.

encapsulated in Ha-PBA$_{69}$-PVA hydrogel exhibited a higher metabolic activity and viability at early time points, likely due to the more favorable oxidative environment. By scavenging ROS and maintaining redox homeostasis, the hydrogel minimized oxidative damage and preserved mitochondrial function. Furthermore, the slight decrease in metabolic activity over time suggests that although ROS levels remained controlled, other factors, such as increased crosslinking density or reduced porosity, may contribute to restricting cell growth and metabolic function limiting nutrient transport and waste removal [76,77]. Together, these results highlight a strong mechanistic link between oxidative microenvironment modulation and downstream cellular outcomes. Thus, optimizing the degree of boronic acid grafting is crucial for simultaneously achieving effective ROS regulation, favorable metabolic activity, and long-term biocompatibility, for the design of Ha-based hydrogels for regenerative medicine applications.

In addition to influencing redox homeostasis and metabolic activity, the degree of PBA grafting also impacted the protein uptake capacity of the hydrogels. As shown in Fig. S7, Ha-PBA-PVA hydrogels, incubated with a 1 mg/mL solution of BSA, showed a marked increase in BSA uptake by Ha-PBA-PVA compared to the control in water, indicating a significant increase in protein-binding capacity. This enhancement was attributed to the intermolecular hydrogen bonding facilitated by the hydroxyl groups of the Ha-PBA-PVA hydrogels, an effect also observed in previous work [78]. Enhanced protein adsorption not only reflects the increased availability of reactive sites in the hydrogel network but also suggests a more bioactive and cell-supportive microenvironment. Proteins adsorbed onto the hydrogel surface or within its matrix can mediate critical biological processes, including cell adhesion, signaling, and nutrient exchange [79], which may further support the higher metabolic activity and viability observed in the 69% grafting formulation.

4. Conclusion

In this study, we developed and characterized ROS-responsive Ha-PBA-PVA hydrogels with tunable degrees of phenylboronic acid grafting and demonstrated their ability to actively modulate the cellular microenvironment. The structural and functional characterization of the Ha-PBA-PVA hydrogels confirmed that tuning the degree of PBA grafting effectively modulated their dynamic properties. Increasing PBA content enhanced crosslink density, yielding hydrogels with higher stiffness and superior elastic recovery, yet exhibiting lower apparent viscosity under shear due to rapid reversible bond exchange. This combination of elasticity at rest and shear-thinning behavior is advantageous for injectability and self-healing. Several ROS-responsive systems have been reported in literature, including antioxidant-loaded matrices, polymer networks and supramolecular macrocycles incorporating redox-sensitive moieties. [80–84]. Compared to these systems, our platform offers a distinctive advantage where mechanical and redox properties can be simultaneously tuned through a single design parameter, namely the degree of PBA grafting. This approach enables precise control over stiffness, viscoelasticity, and antioxidant capacity within the same material system. Furthermore, the use of dynamic boronic ester bonds imparts shear-thinning and self-healing behavior, features that are not universally present in conventional ROS-scavenging hydrogels. While other systems may achieve higher antioxidant loading or more targeted biochemical functionality [80,85], the integration of mechano-redox coupling in a hyaluronic acid-based platform provides a versatile and physiologically relevant model for studying cell–matrix interactions under oxidative stress. Although intracellular ROS levels were assessed to evaluate the antioxidant properties of the hydrogels, the present study does not include an exogenous oxidative stress model. The use of controlled oxidative stimuli, such as hydrogen peroxide exposure, would enable a more direct evaluation of the protective effect of the material under pathological conditions. This represents an important direction for future work, aimed at validating the potential of the hydrogel system to mitigate oxidative stress-induced cellular damage. Moreover, SH-SY5Y cells were employed as a neuron-like model to evaluate cytocompatibility and intracellular ROS modulation within the hydrogel environment. While this model provides a robust and widely used platform for preliminary biological assessment, it does not fully recapitulate the complexity of differentiated neuronal phenotypes. Future studies will aim to incorporate neuronal differentiation protocols or primary neuronal cultures to further investigate the influence of the hydrogel microenvironment on neuronal maturation, functionality, and network formation. The higher-grafted Ha-PBA$_{69}$-PVA formulation most effectively reduced intracellular ROS levels and supported neuronal cell viability, demonstrating that both mechanical and redox properties can be precisely tuned through chemical functionalization. The materials' redox-regulating capacity significantly influenced intracellular ROS levels, which in turn governed cell viability, metabolic activity, and biofunctionality. Hydrogels with higher PBA grafting content exhibited superior antioxidant performance, promoting redox homeostasis, sustaining mitochondrial function, and supporting cell proliferation. Moreover, these hydrogels enhanced protein uptake, suggesting their potential to recruit and present bioactive molecules that further support cellular function.

Specifically, a higher grafting rate creates a more interconnected network, promoting a continuous boronate-mediated reduction of oxidants. This synergy preserves and promotes viability and modulates mitochondrial activity after an initial phase of adaptation. Overall, our results establish the degree of PBA grafting as a single chemical mechanism that regulates network mechanics and ROS reactivity, enabling redox-aware design rules for dynamic Ha-based hydrogels. By explicitly linking chemically measured ROS scavenging to biological modulation of intracellular ROS, this work provides a reproducible approach for designing hydrogels that support the viability of neuronal-like cells by maintaining a compatible redox range for signaling while avoiding persistent oxidative load. These observations can be rationalized by considering the intrinsic reactivity of the PBA moieties within the hydrogel network. PBA moieties are known to exhibit intrinsic reactivity toward ROS, particularly hydrogen peroxide. The ROS-scavenging mechanism is based on the oxidation of the boronic acid group into the corresponding phenolic derivative, resulting in the consumption of ROS species. In the present system, the incorporation of PBA within the hyaluronic acid backbone enabled a dual functionality: first by directing ROS neutralization through chemical reaction with oxidants, and second, by modulating the dynamic boronic ester crosslinks, which are sensitive to oxidative conditions. This coupling between redox activity and network dynamics provided a mechano-redox feedback mechanism, whereby oxidative stimuli can influence both the chemical state and structural organization of the hydrogel as well as the cellular response. At higher grafting degrees, a larger fraction of PBA units participates in dynamic crosslinking, thereby reducing the number of free boronic acid groups available for oxidation. Consequently, hydrogels with lower grafting degrees exhibit slightly higher in vitro hydroxyl radical scavenging, whereas highly grafted systems provide improved control over intracellular ROS, due to a greater overall density of oxidation-susceptible sites distributed throughout the network. By coupling crosslink dependent stiffness/viscoelastic control with arylboronic/boronate ester, our Ha-PBA-PVA hydrogels created a mechano redox microenvironment that stabilized neuronal bioenergetics, providing a microenvironment conducive to neuronal survival and repair. These findings position Ha-PBA-PVA hydrogels as a broadly applicable redox platform for neural bioengineering and in vitro disease modeling.

CRediT authorship contribution statement

Maddalena Grieco: Writing – review & editing, Methodology, Investigation, Formal analysis. **Sara Maria Giannitelli:** Writing – review & editing, Investigation, Formal analysis. **Ilaria Condò:** Investigation, Formal analysis. **Federico Frateloreto:** Investigation, Formal

analysis. **Lorenzo Moroni:** Writing – review & editing. **Marcella Trombetta:** Resources. **Maria Cristina Cannarsa:** Investigation. **Giuseppe Gigli:** Funding acquisition. **Barbara Cortese:** Writing – review & editing, Funding acquisition, Formal analysis, Conceptualization. **Ornella Ursini:** Writing – review & editing, Writing – original draft, Validation, Methodology, Investigation, Formal analysis, Data curation, Conceptualization.

Declaration of competing interest

The authors declare that they have no known competing financial interests or personal relationships that could have appeared to influence the work reported in this paper.

Acknowledgements

The research leading to these results has received funding to the "Tecnopolo per la medicina di precisione" (TecnoMed Puglia) - Regione Puglia: DGR n. 2117 del 21/11/2018, CUP: B84I18000540002 and "Tecnopolo di Nanotecnologia e Fotonica per la medicina di precisione" (TECNOMED) - FISR/MIUR-CNR: delibera CIPE n.3449 del 7-08-2017, CUP: B83B17000010001, and to AIRC under IG 2021 - ID. 26328 project – P.I. Cortese Barbara. The authors are grateful Manuela Marchetti and Giovanna Loffredo a for practical administrative support.

Appendix A. Supplementary data

Supplementary data to this article can be found online at https://doi.org/10.1016/j.bioadv.2026.214913.

Data availability

Data will be made available on request.

References

[1] A. Kumar, J.K. Placone, A.J. Engler, Understanding the extracellular forces that determine cell fate and maintenance, Development 144 (23) (2017 Dec 01) 4261–4270 (PubMed PMID: 29183939. PMCID: PMC5769638. eng).
[2] F. Gattazzo, A. Urciuolo, P. Bonaldo, Extracellular matrix: a dynamic microenvironment for stem cell niche, Biochim. Biophys. Acta 1840 (8) (2014 Aug) 2506–2519 (PubMed PMID: 24418517. PMCID: PMC4081568. Epub 20140110. eng).
[3] H. Geckil, F. Xu, X. Zhang, S. Moon, U. Demirci, Engineering hydrogels as extracellular matrix mimics, Nanomedicine (London) 5 (3) (2010 Apr) 469–484. PubMed PMID: 20394538. PMCID: PMC2892416. eng.
[4] M.W. Tibbitt, K.S. Anseth, Hydrogels as extracellular matrix mimics for 3D cell culture, Biotechnol. Bioeng. 103 (4) (2009 Jul 01) 655–663 (PubMed PMID: 19472329. PMCID: PMC2997742. eng).
[5] V. Muir, J. Burdick, Chemically modified biopolymers for the formation of biomedical hydrogels, Chem. Rev. 121 (18) (2021 SEP 22 2021) 10908–10949. PubMed PMID: WOS:000700878800004. (English).
[6] A. Kirschning, N. Dibbert, G. Dräger, Chemical functionalization of polysaccharides-towards biocompatible hydrogels for biomedical applications, Chemistry 24 (6) (2018 JAN 26 2018) 1231–1240. PubMed PMID: WOS:000423351800002. (English).
[7] D. Diekjürgen, D. Grainger, Polysaccharide matrices used in 3D in vitro cell culture systems, Biomaterials 141 (2017 OCT 2017) 96–115. PubMed PMID: WOS:000406731500009. (English).
[8] O. Ursini, M. Grieco, C. Sappino, A. Capodilupo, S. Giannitelli, E. Mauri, et al., Modulation of methacrylated hyaluronic acid hydrogels enables their use as 3D cultured model, Gels 9 (10) (2023). OCT 2023. PubMed PMID: WOS:001089497400001. (English).
[9] B. Marco-Dufort, M. Tibbitt, Design of moldable hydrogels for biomedical applications using dynamic covalent boronic esters, Mater. Today Chem. 12 (2019 JUN 2019) 16–33. PubMed PMID: WOS:000470901900003. (English).
[10] B. Marco-Dufort, R. Iten, M.W. Tibbitt, Linking molecular behavior to macroscopic properties in ideal dynamic covalent networks, J. Am. Chem. Soc. 142 (36) (2020 Sep 09) 15371–15385 (PubMed PMID: 32808783. Epub 20200831. eng).
[11] S. Huang, X. Kong, Y. Xiong, X. Zhang, H. Chen, W. Jiang, et al., An overview of dynamic covalent bonds in polymer material and their applications, Eur. Polym. J. 141 (2020). DEC 5 2020. PubMed PMID: WOS:000594239600028. (English).
[12] S. Rowan, S. Cantrill, G. Cousins, J. Sanders, J. Stoddart, Dynamic covalent chemistry, Angew. Chem. Int. Ed. Eng. 41 (6) (2002 2002) 898–952. PubMed PMID: WOS:000174450300001. (English).
[13] S. Wanasinghe, O. Dodo, D. Konkolewicz, Dynamic bonds: Adaptable timescales for responsive materials, Angew. Chem. Int. Ed. Eng. 61 (50) (2022 DEC 12 2022). PubMed PMID: WOS:000877677800001. (English).
[14] Y. Han, Y. Cao, H. Lei, Dynamic covalent hydrogels: Strong yet dynamic, Gels 8 (9) (2022). SEP 2022. PubMed PMID: WOS:000857551100001. (English).
[15] F. Picchioni, H. Muljana, Hydrogels based on dynamic covalent and non covalent bonds: a chemistry perspective, Gels 4 (1) (2018). MAR 2018. PubMed PMID: WOS:000461123600020. (English).
[16] I. Condò, S. Giannitelli, D. Lo Presti, B. Cortese, O. Ursini, Overview of dynamic bond based hydrogels for reversible adhesion processes, Gels 10 (7) (2024 JUL 2024). PubMed PMID: WOS:001277535000001. (English).
[17] S. Shahi, H. Roghani-Mamaqani, R. Hoogenboom, S. Talebi, H. Mardani, Stimuli-responsive covalent adaptable hydrogels based on homolytic bond dissociation and chain transfer reactions, Chem. Mater. 34 (2) (2022 JAN 25 2022) 468–498. PubMed PMID: WOS:000768230400001. (English).
[18] M. Rizwan, A.E.G. Baker, M.S. Shoichet, Designing hydrogels for 3D cell culture using dynamic covalent crosslinking, Adv. Healthc. Mater. 10 (12) (2021 Jun) e2100234 (PubMed PMID: 33987970. Epub 20210514. eng).
[19] S. Tang, B. Richardson, K. Anseth, Dynamic covalent hydrogels as biomaterials to mimic the viscoelasticity of soft tissues, Prog. Mater. Sci. 120 (2021 JUL 2021). PubMed PMID: WOS:000674586100001. (English).
[20] E. Aeridou, D. Díaz, C. Alemán, M. Pérez-Madrigal, Advanced functional hydrogel biomaterials based on dynamic B-O bonds and polysaccharide building blocks, Biomacromolecules 21 (10) (2020 OCT 2020) 3984–3996. PubMed PMID: WOS:000580890000003. (English).
[21] A. Pettignano, S. Grijalvo, M. Häring, R. Eritja, N. Tanchoux, F. Quignard, et al., Boronic acid-modified alginate enables direct formation of injectable, self-healing and multistimuli-responsive hydrogels, Chem. Commun. (Camb.) 53 (23) (2017 MAR 21 2017) 3350–3353. PubMed PMID: WOS:000398999000015. (English).
[22] J. Karvinen, M. Kellomäki, Characterization of self-healing hydrogels for biomedical applications, Eur. Polym. J. 181 (2022 DEC 5 2022). PubMed PMID: WOS:000884840800005. (English).
[23] L. Quan, Y. Xin, X. Wu, Q. Ao, Mechanism of self-healing hydrogels and application in tissue engineering, Polymers 14 (11) (2022 JUN 2022). PubMed PMID: WOS:000808993200001. (English).
[24] C. Deng, W. Brooks, K. Abboud, B. Sumerlin, Boronic acid-based hydrogels undergo self-healing at neutral and acidic pH, ACS Macro Lett. 4 (2) (2015 FEB 2015) 220–224. PubMed PMID: WOS:000349814100016. English.
[25] H. Gao, C. Yu, Q. Li, X. Cao, Injectable DMEM-induced phenylboronic acid-modified hyaluronic acid self-crosslinking hydrogel for potential applications in tissue repair, Carbohydr. Polym. 258 (2021). APR 2021. PubMed PMID: WOS:000760325000002. (English).
[26] B.H. Wen Shi, Mitchell A. Kuss, Haipeng Zhang, Sangjin Ryu, Dongze Zhang, Tieshi Li, Yu-long Li, Bin Duan, Fabrication of versatile dynamic hyaluronic acid-based hydrogels, Carbohydr. Polym. 233 (2020) 115803.
[27] C. Schanté, G. Zuber, C. Herlin, T. Vandamme, Chemical modifications of hyaluronic acid for the synthesis of derivatives for a broad range of biomedical applications, Carbohydr. Polym. 85 (3) (2011) 469–489. JUN 1 2011. PubMed PMID: WOS:000291119900001. (English).
[28] Y. Luo, K.R. Kirker, G.D. Prestwich, Cross-linked hyaluronic acid hydrogel films: new biomaterials for drug delivery, J. Control. Release 69 (1) (2000 Oct 03) 169–184 (PubMed PMID: 11018555. eng).
[29] D. Bonneh-Barkay, C.A. Wiley, Brain extracellular matrix in neurodegeneration, Brain Pathol. 19 (4) (2009 Oct) 573–585 (PubMed PMID: 18662234. PMCID: PMC2742568. Epub 20080725. eng).
[30] H. Sivakumar, R. Strowd, A. Skardal, Exploration of dynamic elastic Modulus changes on glioblastoma cell populations with aberrant EGFR expression as a potential therapeutic intervention using a tunable hyaluronic acid hydrogel platform, Gels 3 (3) (2017 Jul 13) (PubMed PMID: 30920523. PMCID: PMC6318698. Epub 20170713. eng).
[31] J.E. Chen, S. Pedron, P. Shyu, Y. Hu, J.N. Sarkaria, B.A.C. Harley, Influence of hyaluronic acid transitions in tumor microenvironment on glioblastoma malignancy and invasive behavior, Front. Mater. 5 (2018 Jun). PubMed PMID: 30581816. PMCID: PMC6300158. Epub 20180626. eng.
[32] M. Carvalho, E. Costa, S. Miguel, I. Correia, Tumor spheroid assembly on hyaluronic acid-based structures: a review, Carbohydr. Polym. 150 (2016) 139–148. OCT vol. 5 2016. PubMed PMID: WOS:000377971800018. English.
[33] A. Fesharaki-Zadeh, Oxidative stress in traumatic brain injury, Int. J. Mol. Sci. 23 (21) (2022 Oct 27) (PubMed PMID: 36361792. PMCID: PMC9657447. Epub 20221027. eng).
[34] Y. Li, X. Xin, X. Zhou, J. Liu, H. Liu, S. Yuan, et al., ROS-responsive biomimetic nanosystem camouflaged by hybrid membranes of platelet-exosomes engineered with neuronal targeting peptide for TBI therapy, J. Control. Release 372 (2024 Aug) 531–50 (PubMed PMID: 38851535. Epub 20240628. eng).
[35] S. Garg, A. Jana, J. Khan, S. Gupta, R. Roy, V. Gupta, et al., Logic "AND gate circuit" based mussel inspired Polydopamine nanocomposite as bioactive antioxidant for Management of Oxidative Stress and Neurogenesis in traumatic brain injury, ACS Appl. Mater. Interfaces 16 (28) (2024 Jul 17) 36168–36193 (PubMed PMID: 38954488. Epub 20240702. eng).
[36] M. Pu, H. Cao, H. Zhang, T. Wang, Y. Li, S. Xiao, et al., ROS-responsive hydrogels: from design and additive manufacturing to biomedical applications, Mater. Horiz. 11 (16) (2024) 3721–3746.
[37] X. Xu, A.K. Jha, D.A. Harrington, M.C. Farach-Carson, X. Jia, Hyaluronic acid-based hydrogels: from a natural polysaccharide to complex networks, Soft Matter 8 (12) (2012) 3280–3294 (PubMed PMID: 22419946. PMCID: PMC3299088. eng).

[38] W. Shi, B. Hass, M. Kuss, H. Zhang, S. Ryu, D. Zhang, et al., Fabrication of versatile dynamic hyaluronic acid-based hydrogels, Carbohydr. Polym. 233 (2020). APR 1 2020. PubMed PMID: WOS:000513914400003. (English).
[39] R. Gao, Z. Yuan, Z. Zhao, X. Gao, Mechanism of pyrogallol autoxidation and determination of superoxide dismutase enzyme activity, Bioelectrochem. Bioenerg. 45 (1) (1998) 41–45. MAR 1998. PubMed PMID: WOS:000074236600006. (English).
[40] X. Li, Improved Pyrogallol autoxidation method: a reliable and cheap Superoxide-scavenging assay suitable for all antioxidants, J. Agric. Food Chem. 60 (25) (2012) 6418–6424. JUN 27 2012. PubMed PMID: WOS:000305716800021. (English).
[41] Y. Zhu, Y. Matsumura, M. Velayutham, L.M. Foley, T.K. Hitchens, W.R. Wagner, Reactive oxygen species scavenging with a biodegradable, thermally responsive hydrogel compatible with soft tissue injection, Biomaterials 177 (2018 Sep) 98–112 (PubMed PMID: 29886387. Epub 20180531. eng).
[42] B. Basilico, M. Grieco, S. D'Amone, I. Palamà, C. Lauro, P. Mozetic, et al., YAP/TAZ cytoskeletal remodelling is driven by mechanotactic and electrotactic cues, Mater. Adv. 6 (1) (2025) 248–262. JAN 3 2025. PubMed PMID: WOS:001367710200001. (English).
[43] Brooks WLA, C.C. Deng, B.S. Sumerlin, Structure-reactivity relationships in boronic acid-diol complexation, ACS Omega 3 (12) (2018 Dec 31) 17863–17870. PubMed PMID: 31458380. PMCID: PMC6644144. Epub 20181219. eng.
[44] P. Chakma, D. Konkolewicz, Dynamic covalent bonds in polymeric materials, Angew. Chem. Int. Ed. 58 (29) (2019 JUL 15 2019) 9682–9695. PubMed PMID: WOS:000476615900002. (English).
[45] W. Brooks, B. Sumerlin, Synthesis and applications of boronic acid-containing polymers: from materials to medicine, Chem. Rev. 116 (3) (2016 FEB 10 2016) 1375–1397. PubMed PMID: WOS:000370216000015. (English).
[46] Y. Guan, Y. Zhang, Boronic acid-containing hydrogels: synthesis and their applications, Chem. Soc. Rev. 42 (20) (2013) 8106–8121.
[47] J. Cash, T. Kubo, A. Bapat, B. Sumerlin, Room-temperature self-healing polymers based on dynamic-covalent boronic esters, Macromolecules 48 (7) (2015 APR 14 2015) 2098–2106. PubMed PMID: WOS:000353176900021. (English).
[48] O. Cromwell, J. Chung, Z. Guan, Malleable and self-healing covalent polymer networks through tunable dynamic boronic ester bonds, J. Am. Chem. Soc. 137 (20) (2015 MAY 27 2015) 6492–6495. PubMed PMID: WOS:000355383500018. (English).
[49] M. Smithmyer, C. Deng, S. Cassel, LeValley P, B. Sumerlin, A. Kloxin, Self-healing boronic acid-based hydrogels for 3D co-cultures, ACS Macro Lett. 7 (9) (2018 SEP 2018) 1105–1110. PubMed PMID: WOS:000445440700010. (English).
[50] S. Budday, R. Nay, R. de Rooij, P. Steinmann, T. Wyrobek, T.C. Ovaert, et al., Mechanical properties of gray and white matter brain tissue by indentation, J. Mech. Behav. Biomed. Mater. 46 (2015 Jun) 318–30 (PubMed PMID: 25819199. PMCID: PMC4395547. Epub 20150302. eng).
[51] M.C. Murphy, J. Huston, C.R. Jack, K.J. Glaser, M.L. Senjem, J. Chen, et al., Measuring the characteristic topography of brain stiffness with magnetic resonance elastography, PLoS One 8 (12) (2013) e81668 (PubMed PMID: 24312570. PMCID: PMC3847077. Epub 20131202. eng).
[52] T. Kaster, I. Sack, A. Samani, Measurement of the hyperelastic properties of ex vivo brain tissue slices, J. Biomech. 44 (6) (2011 Apr 07) 1158–1163. PubMed PMID: 21329927. Epub 20110216. eng.
[53] V. Balbi, A. Trotta, M. Destrade, A. Ní Annaidh, Poynting effect of brain matter in torsion, Soft Matter 15 (25) (2019 Jun 26) 5147–5153 (PubMed PMID: 31192344. eng).
[54] S. Budday, T.C. Ovaert, G.A. Holzapfel, al. e, Fifty shades of brain: a review on the mechanical testing and modeling of brain tissue, Arch Computat Methods Eng (2020) 1187–1230.
[55] E. Holz, K. Rajagopal, In situ-forming glucose-responsive hydrogel from hyaluronic acid modified with a boronic acid derivative, Macromol. Chem. Phys. 221 (15) (2020 AUG 2020). PubMed PMID: WOS:000542880000001. (English).
[56] X. Wu, Z. Li, X. Chen, J. Fossey, T. James, Y. Jiang, Selective sensing of saccharides using simple boronic acids and their aggregates, Chem. Soc. Rev. 42 (20) (2013 2013) 8032–8048. PubMed PMID: WOS:000324888600005. (English).
[57] M. Elsherif, M.U. Hassan, A.K. Yetisen, H. Butt, Glucose sensing with Phenylboronic acid functionalized hydrogel-based optical diffusers, ACS Nano 12 (3) (2018 2018/03/27) 2283–2291.
[58] C. Wang, B. Lin, H. Zhu, F. Bi, S. Xiao, L. Wang, et al., Recent advances in Phenylboronic acid-based gels with potential for self-regulated drug delivery, Molecules 24 (6) (2019 Mar 19) (PubMed PMID: 30893913. PMCID: PMC6470492. Epub 20190319. eng).
[59] S. Parihar, B. Gaur, Self healing approaches in polymeric materials-an overview, J. Polym. Res. 30 (6) (2023 JUN 2023). PubMed PMID: WOS:000993070800002. (English).
[60] M. Regato-Herbella, I. Morhenn, D. Mantione, G. Pascuzzi, A. Gallastegui, A. Valle, et al., ROS-responsive 4D printable acrylic thioether-based hydrogels for smart drug release, Chem. Mater. 36 (3) (2023 DEC 13 2023) 1262–1272. PubMed PMID: WOS:001158811400001. (English).
[61] Q. Zhang, X. Wang, Y. Song, X. Fan, J. García-Martín, Optimization of Pyrogallol autoxidation conditions and its application in evaluation of Superoxide Anion Radical scavenging capacity for four antioxidants, J. AOAC Int. 99 (2) (2016 MAR-APR 2016) 504–511. PubMed PMID: WOS:000374203700024. (English).
[62] A.M. Pisoschi, A. Pop, F. Iordache, L. Stanca, G. Predoi, A.I. Serban, Oxidative stress mitigation by antioxidants - an overview on their chemistry and influences on health status, Eur. J. Med. Chem. 209 (2021 Jan 01) 112891 (PubMed PMID: 33032084. Epub 20200930. eng).
[63] Q. Wang, S. Tian, P. Ning, Degradation mechanism of Methylene Blue in a heterogeneous Fenton-like reaction catalyzed by Ferrocene, Ind. Eng. Chem. Res. 53 (2) (2014 JAN 15 2014) 643–649. PubMed PMID: WOS:000330018500017. (English).
[64] K. Dutta, S. Mukhopadhyay, S. Bhattacharjee, B. Chaudhuri, Chemical oxidation of Methylene Blue using a Fenton-like reaction, J. Hazard. Mater. 84 (1) (2001 JUN 1 2001) 57–71. PubMed PMID: WOS:000169119000004. (English).
[65] Y. Kim, J. Kim, ROS-scavenging therapeutic hydrogels for modulation of the inflammatory response, ACS Appl. Mater. Interfaces 14 (20) (2022 MAY 25 2022) 23002–23021. PubMed PMID: WOS:000737973100001. (English).
[66] P. Wang, Q. Gong, J. Hu, X. Li, X. Zhang, Reactive oxygen species (ROS)-responsive prodrugs, probes, and Theranostic prodrugs: applications in the ROS-related diseases, J. Med. Chem. 64 (1) (2021 Jan 14) 298–325 (PubMed PMID: 33356214. Epub 20201223. eng).
[67] W. Song, J. You, Y. Zhang, Q. Yang, J. Jiao, H. Zhang, Recent Studies on Hydrogels Based on H₂O₂-Responsive Moieties: Mechanism, Preparation and Application, Gels 8 (6) (2022 JUN 2022). PubMed PMID: WOS:000816329000001. (English).
[68] H. Sies, Hydrogen peroxide as a central redox signaling molecule in physiological oxidative stress: Oxidative eustress, Redox Biol. 11 (2017 Apr) 613–619. PubMed PMID: 28110218. PMCID: PMC5256672. Epub 20170105. eng.
[69] H. Sies, D.P. Jones, Reactive oxygen species (ROS) as pleiotropic physiological signalling agents, Nat. Rev. Mol. Cell Biol. 21 (7) (2020 Jul) 363–383 (PubMed PMID: 32231263. Epub 20200330. eng).
[70] B. Liu, Y. Kong, O.A. Alimi, M.A. Kuss, H. Tu, W. Hu, et al., Multifunctional microgel-based cream hydrogels for postoperative abdominal adhesion prevention, ACS Nano 17 (4) (2023 Feb 28) 3847–3864 (PubMed PMID: 36779870. PMCID: PMC10820954. Epub 20230213. eng).
[71] Q. Liu, R. Cong, J. Yu, X. Zhang, J. Tu, Y. Dong, et al., Ros-sensitive hydrogel system incorporating mitochondria-targeted liposomes for periodontitis treatment, Mater. Des. 257 (2025 SEP 2025). PubMed PMID: WOS:001580626500008. (English).
[72] J. Liu, X. Han, T. Zhang, K. Tian, Z. Li, F. Luo, Reactive oxygen species (ROS) scavenging biomaterials for anti-inflammatory diseases: from mechanism to therapy, J. Hematol. Oncol. 16 (1) (2023 Nov 30) 116 (PubMed PMID: 38037103. PMCID: PMC10687997. Epub 20231130. eng).
[73] F.R. Palma, B.N. Gantner, M.J. Sakiyama, C. Kayzuka, S. Shukla, R. Lacchini, et al., ROS production by mitochondria: function or dysfunction? Oncogene 43 (5) (2024 Jan) 295–303 (PubMed PMID: 38081963. Epub 20231211. eng).
[74] E. Kalwarczyk, A. Lukasiak, D. Woznica, W. Switlik, J. Anchimowicz, P. Zielonka, et al., Proliferation of SH-SY5Y neuroblastoma cells on confined spaces, J. Neurosci. Methods 409 (2024 Sep) 110204 (. PubMed PMID: 38925370. Epub 20240624. eng).
[75] A. Ozgun, F.Z. Erkoc-Biradlı, O. Bulut, B. Garipcan, Substrate stiffness effects on SH-SY5Y: the dichotomy of morphology and neuronal behavior, J Biomed Mater Res B Appl Biomater 109 (1) (2021 Jan) 92–101 (PubMed PMID: 32627383. Epub 20200705. eng).
[76] P. Lu, D. Ruan, M. Huang, M. Tian, K. Zhu, Z. Gan, et al., Harnessing the potential of hydrogels for advanced therapeutic applications: current achievements and future directions, Signal Transduct. Target. Ther. 9 (1) (2024 Jul 01) 166 (PubMed PMID: 38945949. PMCID: PMC11214942. Epub 20240701. eng).
[77] S. Asim, E. Hayhurst, R. Callaghan, M. Rizwan, Ultra-low content physio-chemically crosslinked gelatin hydrogel improves encapsulated 3D cell culture, Int. J. Biol. Macromol. 264 (Pt 2) (2024 Apr) 130657. PubMed PMID: 38458282. PMCID: PMC11003839. Epub 20240306. eng.
[78] G. Mandavinia, M. Soleymani, H. Etemadi, M. Sabzi, Z. Atlasi, Model protein BSA adsorption onto novel magnetic chitosan/PVA/Laponite RD hydrogel nanocomposite beads, Int. J. Biol. Macromol. 107 (2018 FEB 2018) 719–729. PubMed PMID: WOS:000423892200081. (English).
[79] S. Zustiak, Y. Wei, J. Leach, Protein-hydrogel interactions in tissue engineering: mechanisms and applications, Tissue Eng. Part B Rev. 19 (2) (2013 APR 2013) 160–171. PubMed PMID: WOS:000315651800006. English.
[80] J. Cao, B. Wu, P. Yuan, Y. Liu, C. Hu, Rational Design of Multifunctional Hydrogels for wound repair, J. Funct. Biomater. 14 (11) (2023 Nov 18) (PubMed PMID: 37998122. PMCID: PMC10672203. Epub 20231118. eng).
[81] Y. Cao, X. Shen, Y. Chen, J. Guo, Q. Chen, X. Jiang, pH-induced self-assembly and capsules of sodium alginate, Biomacromolecules 6 (4) (2005 JUL-AUG 2005) 2189–2196. PubMed PMID: WOS:000230498400050. (English).
[82] J. Wang, Z. Shu, J. Chen, J. Bei, Y. Wu, T. Chen, et al., Target recognition of, Anal. Chem. 97 (49) (2025 Dec 16) 27356–27363 (PubMed PMID: 41345048. Epub 20251204. eng).
[83] Y. Cai, Y. Zhang, X. Liang, C. Deng, J. Zhang, H. Wang, et al., A water-soluble cationic [2]biphenyl-extended pillar[6]arene: synthesis, host-guest interaction with hemin and application in chemodynamic/photodynamic cancer therapy, Chem. Commun. (Camb.) 61 (28) (2025 Apr 01) 5333–5336. PubMed PMID: 40080379. Epub 20250401. eng.
[84] Y. Dai, W. Yu, Y. Cheng, Y. Zhou, J. Zou, Y. Meng, et al., Recent developments in pillar[5]arene-based nanomaterials for cancer therapy, Chem. Commun. (Camb.) 61 (12) (2025 Feb 04) 2484–2495. PubMed PMID: 39789890. Epub 20250204. eng.
[85] S. Zhang, G. Ge, Y. Qin, W. Li, J. Dong, J. Mei, et al., Recent advances in responsive hydrogels for diabetic wound healing, Mater. Today Bio 18 (2023 Feb) 100508. PubMed PMID: 36504542. PMCID: PMC9729074. Epub 20221201. eng.